Study of slowing down mechanism of locked-mode-like instability in helical plasmas

Y. TAKEMURA[1,2], K.Y. WATANABE[1,3], S. SAKAKIBARA[1,2], S. OHDACHI[1,4], Y. NARUSHIMA[1,2], K. IDA[1,2], M. YOSHINUMA[1,2], H. TSUCHIYA[1], T. TOKUZAWA[1], I. YAMADA[1] and LHD EXPERIMENTAL GROUP

[1] National Institute for Fusion Science, National Institutes of Natural Science, Toki, Gifu 509-5292, Japan
[2] SOKENDAI (The Graduate University for Advanced Studies), Toki, Gifu 509-5292, Japan
[3] Nagoya University, Graduate School of Engineering, Chikusa, Nagoya 464-8603, Japan
[4] The University of Tokyo, Graduate School of Frontier Sciences, Kashiwa, Chiba 277-8561, Japan

E-mail: takemura.yuki@nifs.ac.jp

Abstract

The mode slowing down mechanism of the locked-mode-like instability without a large magnetic island is investigated, based on the LHD experimental analysis. The mode frequency coincides with $\boldsymbol{E} \times \boldsymbol{B}$ rotation frequency at the resonant surface and the slowing down is caused by two processes. One is the resonant surface moving to the small $\boldsymbol{E} \times \boldsymbol{B}$ rotation frequency region and the other is the slowing down of the $\boldsymbol{E} \times \boldsymbol{B}$ rotation frequency near the resonant surface. Both processes are almost the same as those of the locked-mode-like instability with a large magnetic island. The results suggest that the slowing down occurs even though the precursor does not have a large magnetic island. However, when the external RMP is imposed, the mode frequency in the slowing down phase sometimes does not coincide with the $\boldsymbol{E} \times \boldsymbol{B}$ rotation frequency. Moreover, the mode amplitude during the slowing down phase increases with the decrease of the mode frequency both with and without the imposed external RMP, which suggests that the instability growth in the slowing down phase is more strongly related to the mode frequency than the $\boldsymbol{E} \times \boldsymbol{B}$ rotation frequency because the mode sometimes does not rotate with the $\boldsymbol{E} \times \boldsymbol{B}$ rotation.

Keywords: MHD instability, locked-mode-like instability, low magnetic shear, mode rotation, LHD, external RMP, locked mode

1. Introduction

The locked-mode-like instability is one of the MHD instabilities observed in the LHD (Large Helical Device) which is the world's largest heliotron [1]. This instability is characterized by the continuous occurrence of the following characteristic behaviour: the dominant fluctuation appears as a precursor, its frequency decreases to zero, the non-rotating magnetic island grows, and the pressure gradient largely degrades [2–5]. Due to such minor collapse, the confinement property seriously deteriorates despite maintaining plasma heating. The minor collapse with the growth of the non-rotating magnetic island is frequently observed in the low magnetic shear region reached by setting to the low magnetic shear configuration and by driving the large co-current due to tangential NBIs (neutral beam injections) [6]. Here, the 'co-' means the direction of the toroidal plasma current to enhance the rotational transform. The precursor sometimes appears before the minor collapse occurs. The minor collapse with the precursor is called the 'locked-mode-like instability' in the LHD because this instability is phenomenally similar to the conventional locked mode in tokamaks [7,8] and RFPs (Reversed Field Pinches) [9]. In order to avoid and suppress the minor collapse, understanding the occurrence mechanism of the minor collapse is important. It is also important to clarify the slowing down mechanism of the precursor which may be related to the minor collapse.

In the LHD, there are two types of the locked-mode-like instability categorized by the difference of the radial structure of the precursor in the slowing down phase. Figure 1 shows the radial structure of the amplitude $\delta I_{\mathrm{ECE}}/I_{\mathrm{ECE}}$ and the phase

difference ϕ_{ECE} of the ECE (Electron Cyclotron Emission) fluctuations due to each instability while the mode frequency decreases. Here, ECE signals are proportional to the electron temperature and these signals are obtained by a multi-channel ECE measurement [10]. The amplitude of the electron temperature fluctuations (δI_{ECE}) due to each instability is normalized by DC component (I_{ECE}) of the electron temperature signals. The reference phase of the ϕ_{ECE} is the phase of the magnetic fluctuation. In Fig. 1 (a), there are two peaks and their phase is inverse. This structure is similar to the tearing-type structure, and thus, this instability is considered to have a large magnetic island. It is called 'type-I instability'. Magnetic island structure of the type-I instability is also observed as characteristic poloidal flow oscillations by a multi-channel Doppler reflectometer [11]. On the other hand, in Fig. 1 (b), there is one peak and the phase near the peak is almost constant. This structure is similar to the interchange-type structure. Therefore, this instability is considered not to have a large magnetic island. It is called 'type-II instability'. The resonant surface is estimated to be located near the inversion surface in the type-I instability and near the peak in the type-II instability. The location of the resonant surface differs between the type-I instability and the type-II instability. Such a difference in the rotational transform profile would be caused by the difference in parameter regime of the type-I instability and the type-II instability. Figure 2 shows the parameter regime where the mode frequency decreases in the diagram of the $<\beta_{dia}>$ and $(d\iota/d\rho)/(\iota/\rho)|_{\iota/2\pi=1}$. Here, $<\beta_{dia}>$ and $(d\iota/d\rho)/(\iota/\rho)|_{\iota/2\pi=1}$ are the volume-averaged beta value and the magnetic shear at the $\iota/2\pi$ = 1 surface, respectively. The slowing down in each instability occurs in the different region. The precursor of the type-I instability slows down in the region of a smaller beta value and a higher magnetic shear compared to the type-II instability. The parameter regime of the slowing type-II precursor is relatively close to the ideal interchange instability regime calculated by linear analysis [12].

The slowing down mechanism of the type-I instability has been discussed in [4] as follows. The frequency of the instability coincides with that of the $\boldsymbol{E} \times \boldsymbol{B}$ rotation frequency at the resonant surface. While the instability slows down, first the resonant surface moves to a small $\boldsymbol{E} \times \boldsymbol{B}$ flow velocity region, and next the $\boldsymbol{E} \times \boldsymbol{B}$ flow velocity near the resonant surface decreases. However, the slowing down mechanism of the type-II instability is still unknown. In this paper, in order to clarify the slowing down process of the type-II instability, the relationship between the frequency of the type-II instability and the $\boldsymbol{E} \times \boldsymbol{B}$ rotation frequency at the resonant surface was investigated.

A rotating magnetic island appears as a precursor of the conventional locked mode in tokamaks and RFPs. It is considered that the slowing down occurs by the electromagnetic torque acting on the plasma due to the interaction between the rotating magnetic island and the external RMP (Resonance Magnetic Perturbation) [13–15]. To clarify the influence of the external RMP on the locked-mode-like instability, the precursor's behaviour of the type-II instability in the discharge with externally imposed RMP of different amplitude was also investigated.

This paper is organized as follows. In Sec. 2, the experimental setup is explained. In Sec. 3, the experimental results of the type-II instabilities are introduced. In Sec.3.1, the slowing down process of the type-II instability is shown through the relationship between the frequency of the precursor and the $\boldsymbol{E} \times \boldsymbol{B}$ rotation frequency at the resonant surface. In Sec. 3.2, the effect of the external RMP is shown. In Sec. 3.3, the relationship between the mode growth and the mode frequency is shown, and the paper is summarized in Sec. 4.

2. Experimental setup

The locked-mode-like instability typically appears in the low magnetic shear regime of the LHD plasmas. The magnetic shear of the whole plasma is lower in the higher aspect ratio configuration when the magnetic axis position in the vacuum magnetic field R_{ax} is set to 3.6 m [16]. In this study, the high aspect ratio A_p of 7.1 is set. In order to observe the radial structure of the internal fluctuations due to the instability by the ECE measurement, the magnetic field strength at the magnetic axis position B_t of 1.3 T is chosen. This is because the radial measurement area of the ECE measurement depends on the B_t and, in case of the B_t ~ 1.3 T, this measurement can obtain the internal fluctuations near the region where the precursor would be localized. In this magnetic configuration, plasmas are produced and maintained by NBIs. The two tangential NBIs drive the large co-current, which further reduces the magnetic shear in whole plasmas, in particular in core region. The perpendicular NBI is modulated to measure the $\boldsymbol{E} \times \boldsymbol{B}$ rotation frequency by the CXS (Charge eXchange Spectroscopy). The CXS signal is obtained while turning on the perpendicular NBI on 40 ms and the background signal is acquired while turning off the NBI on 60 ms. The $\boldsymbol{E} \times \boldsymbol{B}$ rotation frequency is averaged on 40 ms. The sampling time of the $\boldsymbol{E} \times \boldsymbol{B}$ rotation frequency is 100 ms. The precursor can form a flattening region in an electron temperature profile, thus the radial location of the precursor is estimated from the centre of the flattening region in an electron temperature profile measured by the Thomson scattering system. The toroidal and the poloidal mode structure of the fluctuation are identified by a toroidal array with 6 magnetic probes and a helical array with 15 probes outside the plasma [17]. The mode amplitude and the mode frequency are measured by one of the toroidal array probe located ~ 0.3 m away from the $\iota/2\pi$ = 1 surface. To observe the non-rotating magnetic island, the arrays of the saddle loop with the large area enclosed by its loop measures the radial magnetic flux. The averaged area

through which the radial magnetic flux passes is ~ 0.4 m^2. The averaged distance between the saddle loop and the $\iota/2\pi = 1$ surface is ~ 0.5 m. The magnetic shear is measured by the MSE (Motional Stark Effect) diagnostic. The RMP coil system, which consists of 10 vertical pairs of coils at the top and the bottom of the LHD, can cancel the intrinsic error field by imposing external RMP [18]. In this paper, the amplitude of the external RMP is expressed by the normalized RMP coil current I_{RMP}/B_t. For example, the I_{RMP}/B_t is ~ 100 A/T when the intrinsic error field is almost reduced by the external RMP coils. A positive sign of the I_{RMP}/B_t corresponds to the opposite phase to the error field.

3. Experimental results

3.1 Slowing down process of locked-mode-like instability

Figure 3 (a)-(e) show typical waveforms of a discharge with the type-II instability. In this discharge, the I_{RMP}/B_t is ~ 100 A/T, i.e. the intrinsic error field is almost reduced. First of all, the typical behaviour of the precursor is explained. After the precursor with the $m/n = 1/1$ structure appears at t ~ 3.8 s and rotates in the electron diamagnetic direction, the mode frequency f_{mode} and the mode amplitude $\delta b_\theta/B_t$ are almost constant until 4.2 s (constant frequency phase) as shown in Fig. 3 (c) and (d). Then, the f_{mode} gradually decreases and the $\delta b_\theta/B_t$ increases (slowing down phase). Finally, the f_{mode} becomes almost zero at 4.56 s (locking phase). After stopping the mode, amplitude of the radial magnetic fluctuation measured by saddle coils suddenly increases as shown in Fig. 3 (b). This indicates the growth of the non-rotating magnetic island. Note that the $\delta b_\theta/B_t$ and the f_{mode} indicate the amplitude and the frequency of the maximum amplitude Fourier component of the magnetic fluctuation, evaluating by using Wavelet analysis [19]. The sampling time of the $\delta b_\theta/B_t$ and f_{mode} is 10^{-4} s. The f_{mode} seems to have a "width" of the frequency at the same time in rotating phase as shown in Fig. 3 (c). This width is caused by the mode behaviour that the f_{mode} repeatedly increases and decreases in a very short time.

Comparing the f_{mode} with the $\boldsymbol{E} \times \boldsymbol{B}$ rotation frequency at the resonant surface $f_{\boldsymbol{E}\times\boldsymbol{B}}$, the f_{mode} and the $f_{\boldsymbol{E}\times\boldsymbol{B}}$ are almost the same from the constant frequency phase to the slowing down phase, as shown in Fig. 3 (c). It suggests that the precursor rotates with the $\boldsymbol{E} \times \boldsymbol{B}$ plasma flow. Note that a positive sign of Fig. 3 (c) corresponds to an electron diamagnetic direction. By investigating the relationship between the $f_{\boldsymbol{E}\times\boldsymbol{B}}$ profile and the resonant surface location, it is found that the slowing down phase consists of the following two stages. Figure 3 (e) shows the time evolution of the radial profile of the $\boldsymbol{E} \times \boldsymbol{B}$ rotation frequency (filled areas) and the resonant surface location (closed circles). The red (blue) area in Fig. 3 (e) corresponds to the electron (ion) diamagnetic direction. Figure 3 (f) shows the radial profile of the $\boldsymbol{E} \times \boldsymbol{B}$ rotation frequency at three timings. Note that a positive sign of Fig. 3 (f) corresponds to an electron diamagnetic direction. In the first stage, such as t = 4.28 and 4.38 s (red and green lines in Fig. 3 (f)), the resonant surface moves toward the plasma core region (R = 4.16 m to R = 4.06 m), where the $\boldsymbol{E} \times \boldsymbol{B}$ rotation frequency is small. In the second stage (just before t = 4.58 s), the $\boldsymbol{E} \times \boldsymbol{B}$ rotation frequency near the resonant surface becomes small. This behaviour is similar to that of the type-I instability [4].

3.2 Effect of external RMP on locked-mode-like instability

In order to understand the effect of the external RMP on the type-II instability, the behaviour of the type-II instability in the discharges with different amplitude of the residual error field will be shown. The discharges are classified into three types by the effect of the residual error field amplitude on the slowing down phase: almost-reduced error field (I_{RMP}/B_t ~ 100 A/T), half-reduced error field (30 ~ 50 A/T) and less-reduced error field (0 ~ 30 A/T). It should be noted that the experimental condition is almost the same except for the residual error field amplitude. The magnetic configuration is the same and the operational parameter regimes are comparable.

Fig. 4 shows the typical discharge waveforms with the half-reduced error field (Figs. 4 (a) - (c)) and the less-reduced error field (Figs. 4 (d) - (f)). Note that the typical discharge waveform in Fig. 3 corresponds to the almost-reduced error field. Figs. 4 (a) and (d) show the radial magnetic flux amplitude related with the size of the non-rotating magnetic island. Figs. 4 (b) and (e) show the f_{mode} and the $f_{\boldsymbol{E}\times\boldsymbol{B}}$. Figs. 4 (c) and (f) show the mode amplitude. Note that a positive sign of Figs. 4 (b) and (e) correspond to an electron diamagnetic direction. Regardless of the residual error field amplitude, the non-rotating magnetic island grows before the minor collapse (Figs. 3 (b), 4 (a) and (d)). As a further common characteristic, the radial profile of the ECE fluctuations by the type-II instability in the constant frequency phase is an even function type structure across the resonant surface, which is similar to the structure in Fig. 1 (b). In all types of the reduced error field discharge, the discontinuous decrease of the f_{mode} occurs in the slowing down phase. In the beginning of the slowing down phase of the almost-reduced discharges, the frequency of the dominant mode discontinuously drops and then the frequency gradually decreases (Fig. 3 (c)). In the half-reduced and the less-reduced error field discharge, the discontinuous decrease more often occurs and the dominant mode disappears after the discontinuous decrease (Fig. 4 (b) and (e)). As the residual error field amplitude increases, the interval of the discontinuous decrease is longer. In addition, the maximum of the mode amplitude in the slowing down phase is smaller as the residual error field amplitude increases.

In the almost-reduced error field discharges, the mode rotation stops after the $f_{\boldsymbol{E}\times\boldsymbol{B}}$ decreases to almost zero (Fig 3

(c)). On the other hand, in the half-reduced and the less-reduced error field discharges, the mode can lock before the $f_{\boldsymbol{E}\times\boldsymbol{B}}$ drops to zero (Figs. 4 (b) and (e)). The $f_{\boldsymbol{E}\times\boldsymbol{B}}$ at the mode locking ($f_{\boldsymbol{E}\times\boldsymbol{B}\text{ at lock}}$) in the less-reduced error field discharge is larger than that in the half-reduced error field discharge. Here, the $f_{\boldsymbol{E}\times\boldsymbol{B}\text{ at lock}}$ is indicated by arrows of Fig. 4 (b) and (e). The $I_{\mathrm{RMP}}/B_{\mathrm{t}}$ dependence of the $f_{\boldsymbol{E}\times\boldsymbol{B}\text{ at lock}}$ is shown in Fig. 5. The closed circles correspond to the $f_{\boldsymbol{E}\times\boldsymbol{B}\text{ at lock}}$ and the cross symbols correspond to the averaged value of the $f_{\boldsymbol{E}\times\boldsymbol{B}\text{ at lock}}$ at each $I_{\mathrm{RMP}}/B_{\mathrm{t}}$. The variation in the $f_{\boldsymbol{E}\times\boldsymbol{B}\text{ at lock}}$ is large, but as the residual error field amplitude increases, the averaged value of the $f_{\boldsymbol{E}\times\boldsymbol{B}\text{ at lock}}$ approaches zero. However, the averaged value is not completely zero in the almost-reduced error field discharge. This may be caused by the overestimating $f_{\boldsymbol{E}\times\boldsymbol{B}\text{ at lock}}$ and/or lack of the measurement accuracy of the $f_{\boldsymbol{E}\times\boldsymbol{B}}$ below 300 Hz. Since the $f_{\boldsymbol{E}\times\boldsymbol{B}\text{at lock}}$ is evaluated by linear interpolation of the $f_{\boldsymbol{E}\times\boldsymbol{B}}$ with the sampling time of 100 ms, the $f_{\boldsymbol{E}\times\boldsymbol{B}\text{ at lock}}$ may be overestimated in the situation where $f_{\boldsymbol{E}\times\boldsymbol{B}}$ is zero before the measurement time.

The effect of the external RMP on the duration time of the slowing down phase $\Delta t_{\mathrm{slowing}}$ is also investigated. Usually, $\Delta t_{\mathrm{slowing}}$ is defined as the time from the start of the decrease of the f_{mode} until the f_{mode} reaches almost zero. However, it is difficult to evaluate the slowing down phase from the f_{mode} because the f_{mode} in the slowing down phase discontinuously decreases as shown in Fig. 4 (b) and (e). Therefore, another definition of the $\Delta t_{\mathrm{slowing}}$ is required. Figure 6 (a) and (b) show the f_{mode} and the radial mode amplitude $\delta\Phi_{\mathrm{r,m=1}}/B_{\mathrm{t}}$ in the almost-reduced error field discharge. There are some spikes in the $\delta\Phi_{\mathrm{r,m=1}}/B_{\mathrm{t}}$ and the first spike occurs when the mode starts to slows down. Therefore, the first spike could be an indicator of the start of the slowing down phase. Also in the half-reduced and the less-reduced error field discharge, the spikes also appear as shown in Fig. 6 (c) and (d). The $\Delta t_{\mathrm{slowing}}$ is defined as the period between the time when the first spike appears and that when the non-rotating magnetic island grows. The $I_{\mathrm{RMP}}/B_{\mathrm{t}}$ dependence of the $\Delta t_{\mathrm{slowing}}$ is summarized in Fig. 7. The duration time is the longest in the almost-reduced error field discharges and the duration time becomes shorter as the residual error field amplitude increases. This may be because the $f_{\mathrm{mode\ at\ lock}}$ is larger as the residual error field amplitude more increases as shown in Fig. 5.

3.3 Relationship between mode growth and mode frequency

It seems that the mode amplitude is correlated with both the f_{mode} and the $f_{\boldsymbol{E}\times\boldsymbol{B}}$ in the slowing down phase of the almost-reduced error field discharges where the f_{mode} is almost the same as the $f_{\boldsymbol{E}\times\boldsymbol{B}}$. On the other hand, the previous section shows that there is a difference between the f_{mode} and the $f_{\boldsymbol{E}\times\boldsymbol{B}}$ in the half-reduced and the less-reduced error field discharges, in particular, near the locking phase. In this section, by using this characteristic, it will be shown which frequency of the f_{mode} or the $f_{\boldsymbol{E}\times\boldsymbol{B}}$ the mode amplitude more correlates with.

Figure 8 shows the time evolution of the f_{mode} and the mode amplitude in the slowing down phase of the half-reduced error field discharge. The time-averaged frequency gradually decreases. However, in a short term the f_{mode} sometimes decreases and in the other times increases. For example, at 4.22 s, the f_{mode} abruptly drops to 0.8 kHz. After that, the f_{mode} turns to increase to 2 kHz. When the f_{mode} suddenly drops, the mode amplitude rapidly increases once, and then the mode amplitude turns to decrease as the f_{mode} increases. Such behaviour is observed regardless of the residual error field amplitude. This result suggests that there is a strong correlation between the mode amplitude and the f_{mode} except for data just after the f_{mode} suddenly drops as shown in the hatched region in Fig. 8. The mode behaviour with a strong negative correlation between the mode frequency and the mode amplitude is maintained much longer than that without a strong negative correlation just after the f_{mode} suddenly drops (the hatched areas). Therefore, the mode behaviour with the strong negative correlation is typical. The increase of the f_{mode} after rapid drop of the f_{mode} suggests that the mode rotation accelerates in order to follow the $f_{\boldsymbol{E}\times\boldsymbol{B}}$ because the f_{mode} just before rapid drop almost coincides with the $f_{\boldsymbol{E}\times\boldsymbol{B}}$ as shown in Figs. 4 (b) and (e).

Fig. 9 shows the systematic summary of the f_{mode} and the mode amplitude in the slowing down phase of the almost-reduced discharges (red symbols), and the half-reduced and the less-reduced error field discharges (blue symbols). Here, note that the light blue (light red) symbols indicate data just after rapid drop of the f_{mode} in the $I_{\mathrm{RMP}}/B_{\mathrm{t}} \leq 50$ A/T discharge (the almost-reduced error field discharge). There is a strong correlation between the mode amplitude and the f_{mode} except for data just after the f_{mode} suddenly drops regardless of the residual error field amplitude, which suggests that the f_{mode} more strongly contributes to the mode growth rather than the the $f_{\boldsymbol{E}\times\boldsymbol{B}}$ because there is a difference between the f_{mode} and the $f_{\boldsymbol{E}\times\boldsymbol{B}}$ in the $I_{\mathrm{RMP}}/B_{\mathrm{t}} \leq 50$ A/T discharges as shown in Figs 4 (b), (e) and Fig. 5. In addition, the mode amplitude at a specific frequency in the $I_{\mathrm{RMP}}/B_{\mathrm{t}} \leq 50$ A/T discharge (the effective external RMP amplitude is large) is smaller than that in the almost-reduced error field discharge (the effective external RMP amplitude is small). Therefore, the type-II instability may be stabilized by the total external RMP which is composed of the external RMP by the RMP coil system and the error field.

4. Summary

In order to clarify the physical mechanism by which the locked-mode-like instability observed in the LHD leads to minor collapse, the slowing down mechanism of the instability, which may be related to the occurrence of minor collapse, has been investigated through the experimental analysis. Two

types of the locked-mode-like instability (type-I with a magnetic island and type-II without a magnetic island) are observed in the LHD. In this paper, the slowing down mechanism of the type-II instability is investigated. First, it is found that the precursor rotates with the $\boldsymbol{E} \times \boldsymbol{B}$ flow at the resonant surface because the f_{mode} is almost the same as the $f_{\boldsymbol{E} \times \boldsymbol{B}}$. Next, the slowing down process has the following two stages: (1) the stage where the resonant surface moves to the region where the $\boldsymbol{E} \times \boldsymbol{B}$ rotation frequency is small and (2) where the radial profile of the $\boldsymbol{E} \times \boldsymbol{B}$ rotation frequency near the resonant surface is largely changed. Such a slowing down process is similar to that of the type-I instability with a magnetic island. This result suggests that the effect of the magnetic island size on the slowing down of the locked-mode-like instability in the LHD is not significant.

In addition, the effect of the residual error field on the type-II instability is investigated by comparing the behaviour of the type-II instability in the discharges with the residual error field of various amplitude. It is found that as the external RMP amplitude increases, the mode frequency does not follow the $\boldsymbol{E} \times \boldsymbol{B}$ rotation frequency at the resonant surface, the interval of the discontinuous decrease is longer and the duration time of the slowing down phase becomes shorter.

Furthermore, by investigating the relationship between the precursor's amplitude and the precursor's frequency in the slowing down phase through the systematic analysis, it is found that the amplitude becomes larger as the mode frequency decreases. There is such a strong correlation regardless of the residual error field amplitude. Since the precursor does not rotate with the $\boldsymbol{E} \times \boldsymbol{B}$ rotation in the half-reduced and the less-reduced discharges, it is suggested that the mode growth is strongly related to the decrease of the mode frequency rather than to the reduction of the $\boldsymbol{E} \times \boldsymbol{B}$ rotation frequency. Therefore, it is difficult to stabilize the locked-mode-like instability in the half-reduced and the less-reduced discharges by controlling the plasma flow. For the stabilization by the plasma flow, the cancellation of the intrinsic error field is important.

Finally, a conceptual diagram summarizing typical characteristics is shown in Fig. 10. Figs. 10 (a) and (b) show the mode frequency and the mode amplitude in log scale in the discharge with almost-reduced error field. Figs. 10 (c), (d) show same parameters as Figs. 10 (a), (b), but with the half-reduced error field. Figs. 10 (e), (f) show same parameters as Figs. 10 (a), (b), but with the less-reduced error field. Here, the hatched area corresponds to data just after the mode frequency rapidly drops. Open circles show the $f_{\boldsymbol{E} \times \boldsymbol{B}}$ at the growth of the non-rotating magnetic island. Closed circles indicate measurement data of $f_{\boldsymbol{E} \times \boldsymbol{B}}$ and dashed line through closed circles indicates linearly interpolating of measurement data.

Acknowledgements

This work was supported in part by JSPS KAKENHI (No.25289342), by NIFS under constracts NIFS07KLPH004 and by a dispatch grant from the Future Energy Research Association. The authors are grateful to the LHD Operation Group for their excellent technical support.

References

[1] Takeiri Y. *et al* 2017 *Nucl. Fusion* **57** 102023
[2] Takemura Y. *et al* 2012 *Nucl. Fusion* **52** 102001
[3] Sakakibara S. *et al* 2015 *Nucl. Fusion* **55** 083020
[4] Takemura Y. *et al* 2017 *Plasma Fusion Res.* **12** 1402028
[5] Sakakibara S. *et al* 2013 *Nucl. Fusion* **53** 043010
[6] Sakakibara S. *et al* 2006 *Fusion Sci. Technol.* **50** 177–85
[7] ITER Physics Expert Group on Disruptions *et al* 1999 Chapter3: MHD stability, operational limits and disruptions *Nucl. Fusion* **39** 2251
[8] Hender T.C. *et al* 2007 Progress in the ITER Physics Basis Chapter 3: MHD stability, operational limits and disruptions *Nucl. Fusion* **47** S128
[9] Brunsell P.R. *et al* 1993 *Phys. Fluids* B **5** 885–95
[10] Tokuzawa T. *et al* 2010 *Fusion Sci. Technol.* **58** 364–74
[11] Tokuzawa T. *et al* 2017 *Nucl. Fusion* **57** 076003
[12] Watanabe K.Y. *et al* 2018 Study of interchange MHD instability in low magnetic shear heliotron plasma with net toroidal current *27th Int. Toki Conf. (Toki, Japan, November2018)* P2-02
[13] Zohm H. *et al* 1990 *Europhys. Lett.* **11** 745–50
[14] Hender T.C. *et al* 1992 *Nucl. Fusion* **32** 2091–117
[15] Buttery R.J. *et al* 1999 *Nucl. Fusion* **39** 1827–35
[16] Watanabe K.Y. *et al* 2010 *Fusion Sci. Technol.* **58** 160–75
[17] Sakakibara S. *et al* 2010 *Fusion Sci. Technol.* **1055** 471–81
[18] Morisaki T. *et al* 2010 *Fusion Sci. Technol.* **58** 465–70
[19] Torrence C. and Compo G.P. 1998 *Bull. Am. Meteorol. Soc.* **79** 61

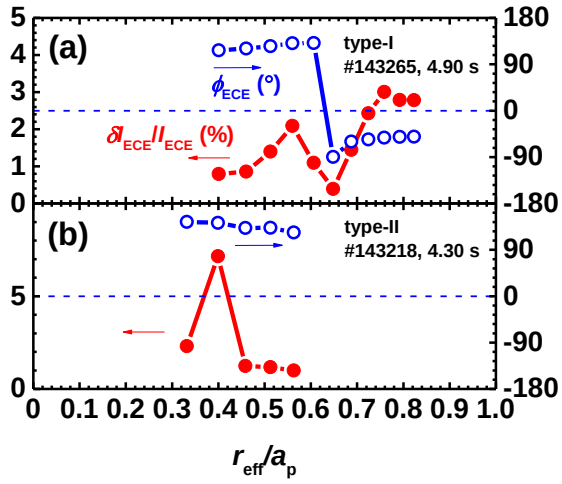

Figure 1. The radial structure of the amplitude $\delta I_{ECE}/I_{ECE}$ and the phase difference ϕ_{ECE} of the electron temperature fluctuations by (a) the type-I instability and (b) the type-II instability while the mode frequency decreases. Here, r_{eff} is the minor radius and a_p is the plasma minor radius.

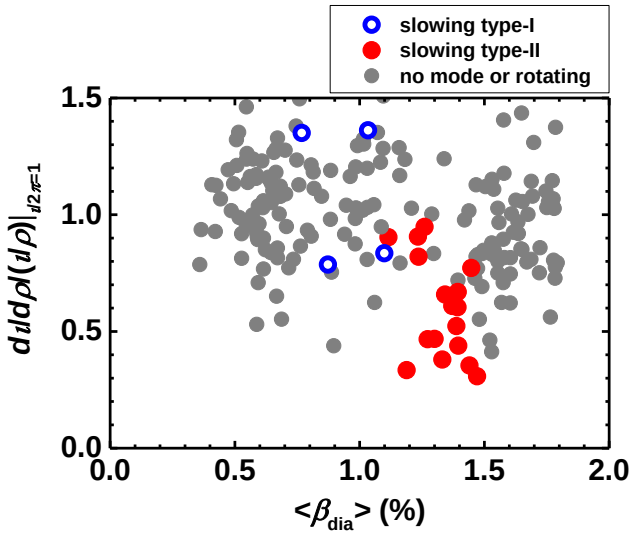

Figure 2. The parameter regime where the precursor slows down in the diagram of the beta value $<\beta_{dia}>$ and the magnetic shear at $\iota/2\pi = 1$ surface $(d\iota/d\rho)/(\iota/\rho)|_{\iota/2\pi=1}$. Grey symbols correspond to the regime where the precursor does not appear or where the precursor rotates at an almost constant frequency. Blue open circles (red closed circles) correspond to the regime where the precursor slows down in the type-I (type-II) instability.

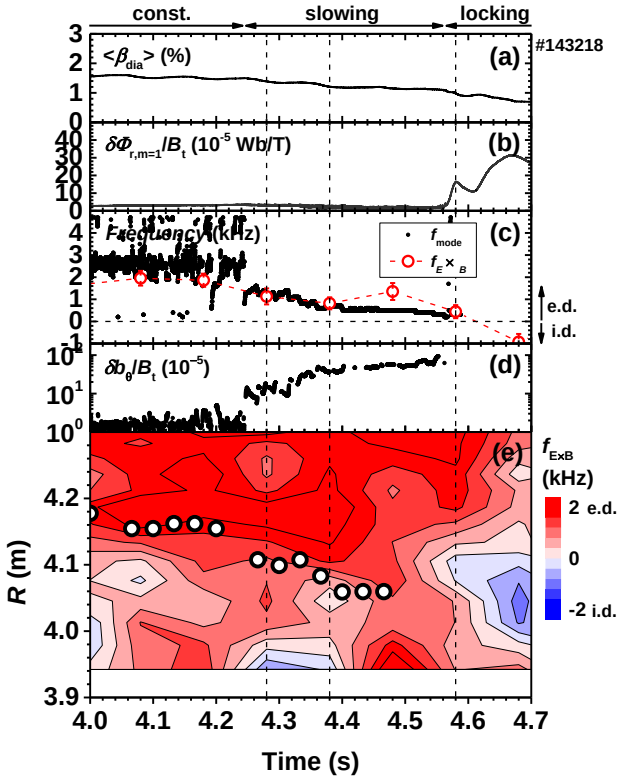

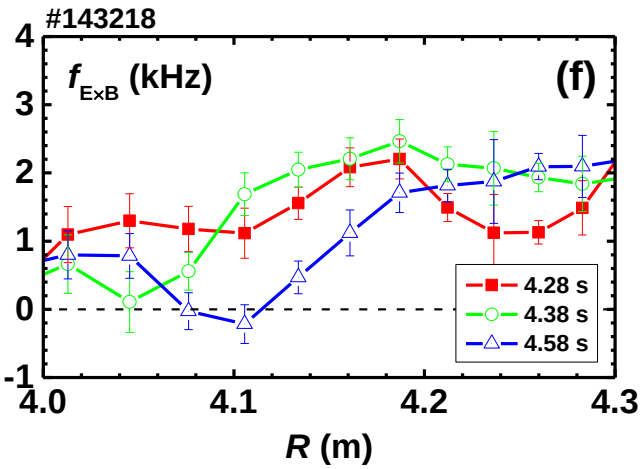

Figure 3. Time evolution of (a) volume-averaged beta value, (b) radial mode amplitude by saddle loop coils, (c) mode frequency f_{mode} by a magnetic probe (closed circles) and $\boldsymbol{E} \times \boldsymbol{B}$ rotation frequency $f_{\boldsymbol{E}\times\boldsymbol{B}}$ at $\iota/2\pi = 1$ resonant surface (open circles), (d) poloidal mode amplitude by a magnetic probe and (e) radial profile of $\boldsymbol{E} \times \boldsymbol{B}$ rotation frequency and location of $\iota/2\pi = 1$ resonant surface (closed circles). (f) radial profile of $\boldsymbol{E} \times \boldsymbol{B}$ rotation frequency at each time corresponding to vertical lines in Figs. 3 (a)-(e) in the almost-reduced error field discharge. A positive (negative) sign of Fig. 3 (c) and (f) means an electron (ion) diamagnetic direction. The red (blue) area in Fig. 3 (e) corresponds to the electron (ion) diamagnetic direction.

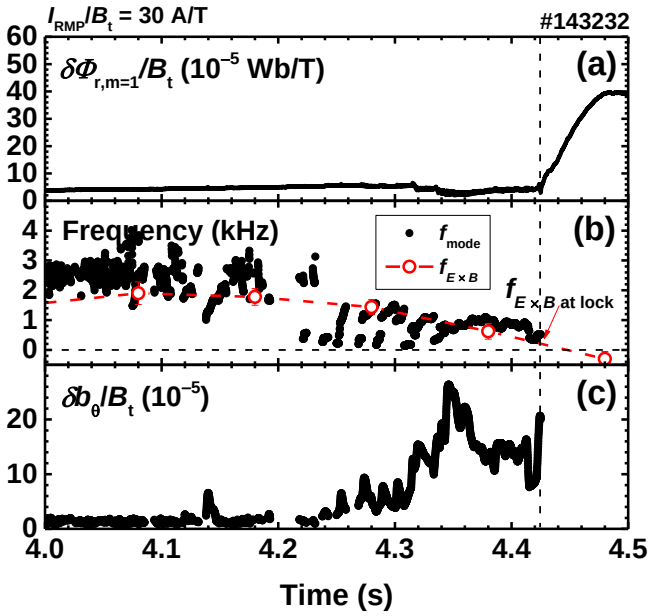

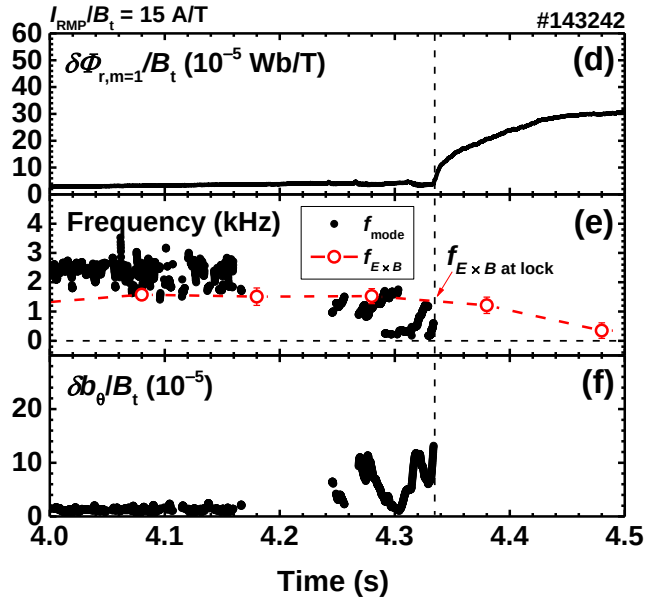

Figure 4. Typical discharge waveforms of the type-II instability with residual error field. (a) radial mode amplitude by saddle loop coils, (b) mode frequency by a magnetic probe, and (c) poloidal mode amplitude in the discharge with the half-reduced error field. Figs 4 (d)-(f) show the same parameters as Figs. 4(a)-(c), but with less-reduced error field. Dashed line indicates the time when the non-rotating magnetic island grows.

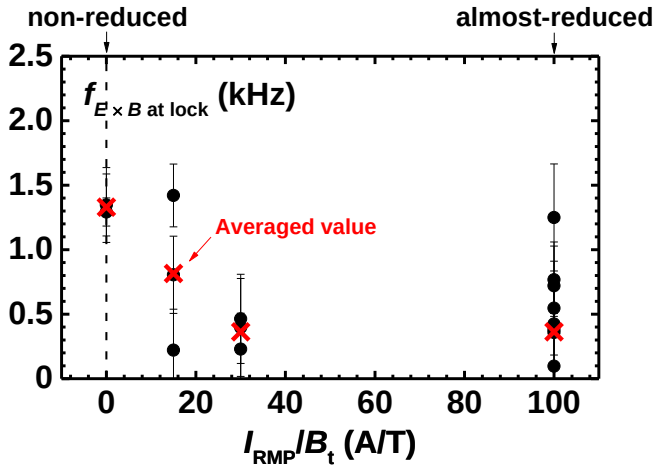

Figure 5. The I_{RMP}/B_t dependence of the $f_{E\times B}$ when the non-rotating magnetic island grows. The closed circles correspond to the $f_{E\times B\ at\ lock}$ and the cross symbols correspond to the averaged value of the $f_{E\times B\ at\ lock}$ at each IRMP/Bt.

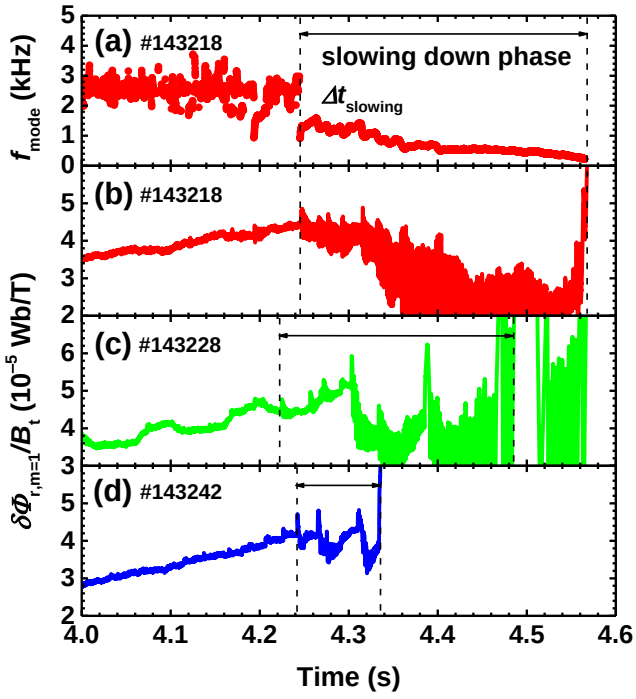

Figure 6. (a) The mode frequency in the almost-reduced error field discharge, (b) radial mode amplitude in the same discharge as Fig. 6 (a), (c) in the half-reduced error field discharge, and (d) in the less-reduced error field discharge.

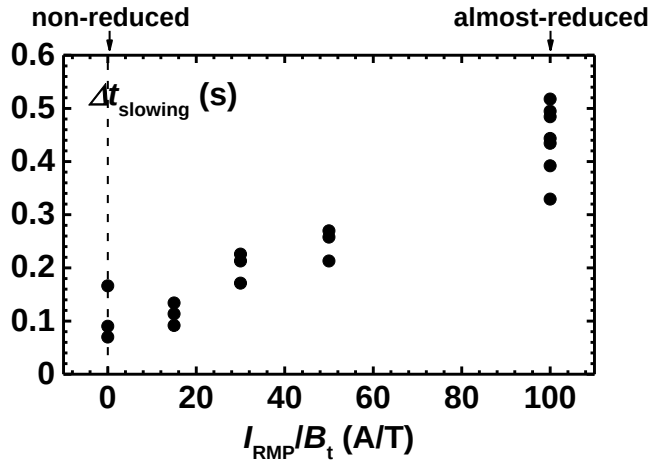

Figure 7. The I_{RMP}/B_t dependence of the duration time of the slowing-down phase $\Delta t_{slowing}$.

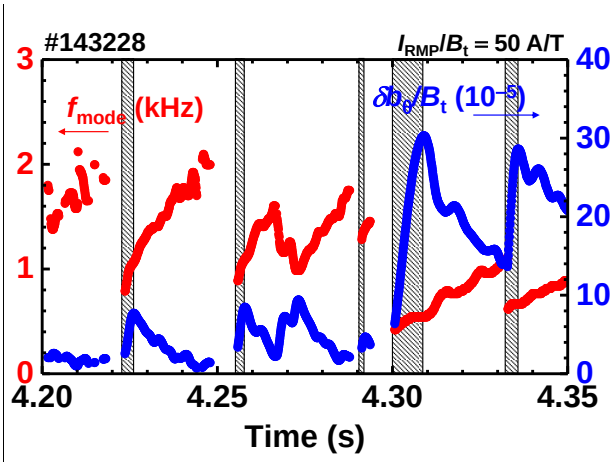

Figure 8. Time evolution of the mode frequency and the mode amplitude in the slowing down phase in the half-reduced error field discharge. The hatched areas indicate the time just after the mode frequency rapidly drops.

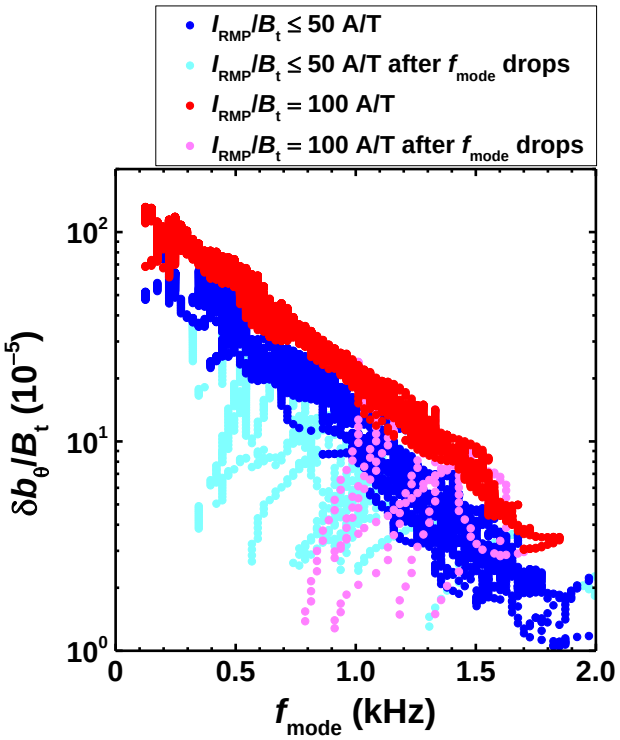

Figure 9. Relationship between the mode amplitude $\delta b_\theta/B_t$ and the mode frequency f_{mode} in the slowing down phase of the $I_{RMP}/B_t \leq$ 50 A/T and the almost-reduced error field discharge. It should be noted that the mode amplitude is shown in log scale. Light blue (light red) symbols indicate data at the time just after the mode frequency rapidly drops in the $I_{RMP}/B_t \leq$ 50 A/T discharge (the almost-reduced error field discharge).

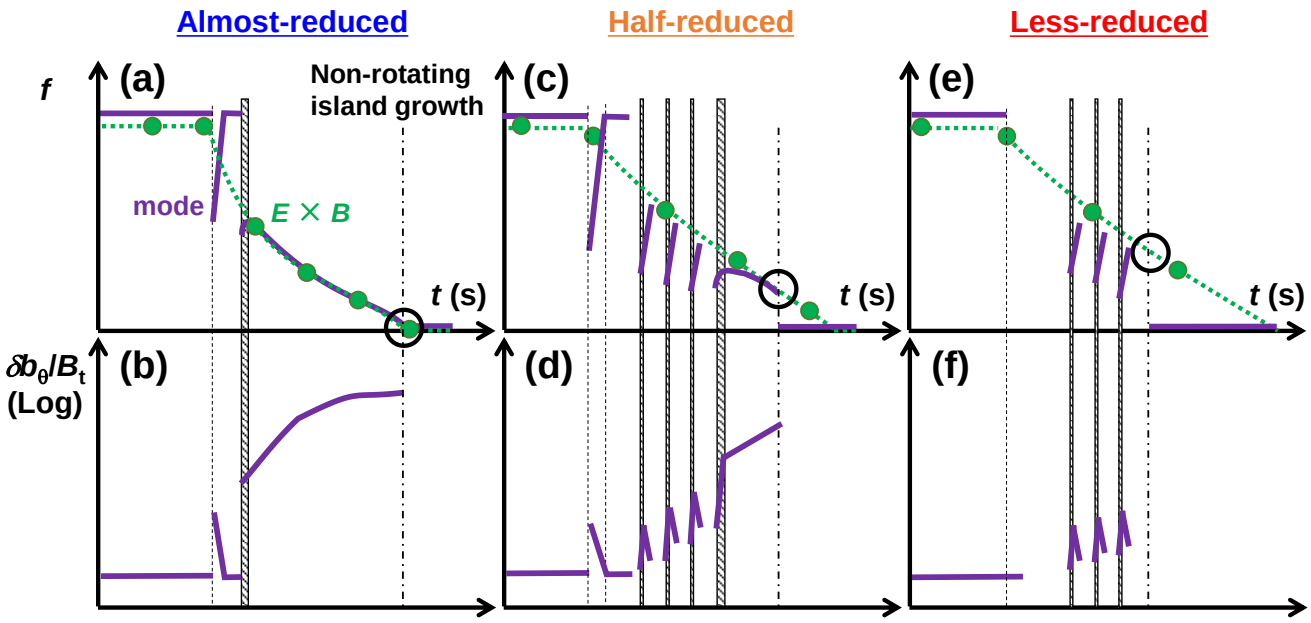

Figure 10. Conceptual diagrams of typical behaviour of the type-II instability. (a) mode frequency and (b) mode amplitude in log scale in the almost-reduced error field discharge. Figs. 10 (c) and (d) show same parameters as Figs. 10 (a) and (b), but with the half-reduced error field. Figs. 10 (e) and (f) show same parameters as Figs. 10 (a) and (b), but with the less-reduced error field. The hatched regions indicate data at the time just after the mode frequency rapidly drops. Open circles show the $f_{E \times B}$ at the growth of the non-rotating magnetic island. Closed circles indicate measurement data of $f_{E \times B}$ and dashed line through closed circles indicates linearly interpolating of measurement data.